Carbon Neutrality

ORIGINAL ARTICLE

Open Access

$Na_5YSi_4O_{12}$ fast ion conductor protection layer enabled dendrite-free Zn metal anode

Ningbo Xu[1†], Chenbo Yuan[1†], Ge Sun[1], Nan Chen[1], Shiyu Yao[1*] and Fei Du[1*]

Abstract

Aqueous zinc-ion batteries (AZIBs) are promising for future large-scale energy storage systems, however, suffer from inferior cycling life due to the dendrites growth and side reaction on Zn metal anode. Herein, a fast ion conductor $Na_5YSi_4O_{12}$ (NYSO) was synthesized and fabricated as a protection layer of the Zn metal anode. By adjusting the thickness, an optimized NYSO coating of 20.3 μm was obtained and the corresponding symmetry cell demonstrates an extended life span of 1896 h at the current density of 0.5 mA cm^{-2}. In addition, a favorable rate performance of the NYSO@Zn anode at a high current density of 10 mA cm^{-2} was achieved. Benefiting from the NYSO coating, uniform diffusion and deposition of Zn^{2+} on the Zn anode could be realized, leading to the elimination of Zn dendrites and side reactions. Therefore, the aqueous NYSO@Zn|CNT@MnO_2 full cell shows superior capacity and cycling stability to that of the bare Zn full cell.

Keywords Aqueous zinc-ion batteries, Zinc metal anode, Fast ion conductor, Interfacial protective layer

1 Introduction

Due to the unique benefits of Zn metal anodes, such as their high abundance, aqueous solution reaction environment, suitable electrochemical potential (-0.762 V vs SHE), high volumetric capacity (5855 mA h cm^{-3}), and specific capacity (820 mA h g^{-1}), aqueous zinc-ion batteries (AZIBs) have recently attracted a lot of attention [1–4]. However, Zn anodes face the challenge of dendrite growth, which can lead to low coulombic efficiency (CE), poor cycling stability, and short-circuiting [5–8]. In addition to this, side effects (hydrogen precipitation), zinc corrosion, and formation of irreversible discharging substances during charging and discharging have seriously hindered the practical application of zinc anodes [9–11]. Worse still, dendrite formation and side reactions are mutually supportive during electrochemical reactions: side reactions change the distribution of electric fields and ions on the surface, resulting in new dendrite growth sites; localized dendrite growing areas have higher loading concentrations and more active sites, which can catalyze the activity of side reactions. Resolving zinc dendrites is an inevitable process for large-scale applications of rechargeable batteries, so proposing an effective strategy is a critical step.

So far, various strategies, such as the structural design of Zn metal anode [12–15], utilization of electrolyte additives [16–18] and incorporation of interfacial protective layers [19–21], have been proposed to optimize and stabilize the Zn metal anode. Among them, introducing a functional protective layer is considered the most straightforward and efficient way to improve the reversibility of Zn anode. By simply coating Zn anode with different materials, the direct contact between Zn and the aqueous electrolyte could be avoided, therefore alleviating the side reactions, such as corrosion and hydrogen evolution. More importantly, uniform deposition of Zn could be achieved by homogenizing the

†Ningbo Xu and Chenbo Yuan contributed equally to this work.

*Correspondence:
Shiyu Yao
yaoshiyu@jlu.edu.cn
Fei Du
dufei@jlu.edu.cn
[1] Key Laboratory of Physics and Technology for Advanced Batteries (Ministry of Education), State Key Laboratory of Superhard Materials, College of Physics, Jilin University, Changchun 130012, China

interfacial electric field or ion distribution with electron or ion-regulating materials, leading to dendrite-free Zn anodes [22]. For example, inorganic materials like $CaCO_3$ [23], ZrO_2 [24], kaolin [25], Zn-based montmorillonite [26], and Mg–Al layered double hydroxide [27], etc., have been demonstrated to prolong the cycling life of Zn anode, by producing uniform zinc ion flux on the surface of Zn metal [28–30]. In particular, fast ion conductor, $NaTi_2(PO_4)_3$ (NTP) [31] has been reported as a solid-state electrolyte protection layer to enable internal transport/mobility of Zn^{2+} like an "ion passable fence". The NTP layer prevents the zinc dendrites and exhibits superlong cycling life, which suggests that the fast ion conductor could be a promising material for the interfacial engineering of Zn metal anode. However, the work evolving fast ion conductors for Zn anode protection is still limited and needs to be further explored in stabilizing the Zn metal anode.

Inspired by the application of NTP, herein, a fast ion conductor $Na_5YSi_4O_{12}$ (NYSO) was developed as a protection layer to promote the electrochemical properties of the Zn metal anode. With an NYSO coating of 20.3 μm, the Zn metal anode demonstrates an extended life span of 1896 h at the current density of 0.5 mA cm^{-2}. In addition, the NYSO@Zn anode presents a favorable rate performance at a high current density of 10 mA cm^{-2}. The superior reversibility of NYSO@Zn anode could be attributed to the elimination of Zn dendrites and side reaction by-products $ZnSO_4(OH)_6{\cdot}5H_2O$. Therefore, an aqueous NYSO@Zn|CNT@MnO_2 full cell delivers superior capacity and stability to that of a bare Zn battery system.

2 Results and discussion

The schematic crystal structure of $Na_5YSi_4O_{12}$ is shown in Fig. 1a, which is composed of SiO_4 tetrahedra linked to form puckered $Si_{12}O_{36}$ rings stacking to form large rigid columns parallel to the *c* axis. $Na_5YSi_4O_{12}$ is synthesized as in previous reports, and the detailed synthesis process is presented in the experimental section. The X-ray Diffraction (XRD) pattern shows that all the diffraction peaks are readily assigned to $Na_5YSi_4O_{12}$ (JCPDS Card No. 32–1204) (Fig. 1b). The SEM image of $Na_5YSi_4O_{12}$ (Fig. 1c) presents the morphology of the micro-sized bulk material. The $Na_5YSi_4O_{12}$ coating layers are successfully prepared on the Zn metal anode by using a controllable thickness coater, here a high-energy ball mill is also used to reduce the particle size. The electrochemical performance of the bare Zn and NYSO@Zn electrodes with different coater thicknesses of 20 μm, 50 μm, 100 μm and 200 μm are investigated in the symmetric cell by repeated plating/peeling measurements at 1 mA cm^{-2} (Fig. 1d). After 130 h of stripping/plating, a sudden voltage drop was detected, which is attributed to a short circuit caused by the Zn dendrites, resulting in failure for the bare Zn cell. In contrast, all NYSO@Zn symmetric cells could sustain repeated deposition/dissolution processes without obvious significant fluctuations over 200 h, indicating improved anode stability. As displayed in Figure S1, NYSO@Zn symmetric cells show high dependence on the NYSO thickness and exhibit the smallest polarization voltage of 28 mV when the coater thickness is set to 50 μm. The lowest charge transfer resistance is also observed in the same coater thickness of 50 μm, suggesting efficient interfacial kinetics, which may promote a relatively uniform metal plating process (Fig. 1e). The scanning electron microscopy (SEM) image of $Na_5YSi_4O_{12}$ layer with coater thickness of 50 μm shows a uniform and dense morphology of $Na_5YSi_4O_{12}$ (Fig. 1f). The uniform distribution of the Na, Y, Si and O elements in energy-dispersive X-ray spectroscopy (EDS) mapping further confirms the compact coverage of $Na_5YSi_4O_{12}$ covering the Zn anode (Fig. 1g-j). The cross-sectional SEM imaging shows a real thickness of 20.3 μm when the coater thickness is 50 μm, due to the evaporation of solvents (Fig. 1k).

To evaluate the anode stability, the long-term electrochemical performance of the bare Zn and NYSO@Zn symmetric cells were tested at different current densities of 0.5, 1, 2 and 5 mA cm^{-2} for 0.5 mAh cm^{-2} respectively. Cycled at 1.0 mA cm^{-2} with 0.5 mA h cm^{-2}, the short-circuit induced premature failure occurs for the symmetric cell with bare Zn after 500 h. By contrast, the NYSO@Zn electrode shows ultralow voltage hysteresis (≈30 mV) with negligible voltage oscillation and ultralong lifespan of 1896 h (Fig. 2a). Under an elevated current density of 1 mA cm^{-2}, the NYSO@Zn symmetric cell shows prolonged cycling life of 1270 h, which is 9 times that of the bare Zn anode (Figure S2). Besides, comparing the initial surface, the bare Zn suffers deep corrosion and chaos dendrite formation after 100 cycles, whereas the NYSO@Zn maintains even surface morphology, much attributing to the NYSO layer's ability to restrain the attack of H_2O and realize even Zn^{2+} transport flux (Figure S3). The bare Zn symmetric cells experience more rapid failure and show short circuits at cycling times less than 100 and 25 h in 2 and 5 mA cm^{-2}, which might be due to the rampant Zn dendrites growth at high current densities. However, the NYSO@Zn anodes display smaller overpotentials and stable cycle life up to 1418 and 385 h at 2 and 5 mA cm^{-2} as shown in Figs. 2b and S4. In addition, the enlarged voltage–time curves of NYSO@Zn symmetric cells deliver a smaller polarization than those of bare Zn at 0.5 and 2 mA cm^{-2} (Figure S5). These results indicate that $Na_5YSi_4O_{12}$ coating can achieve uniform Zn^{2+} deposition to avoid dendrite formation and extend battery life.

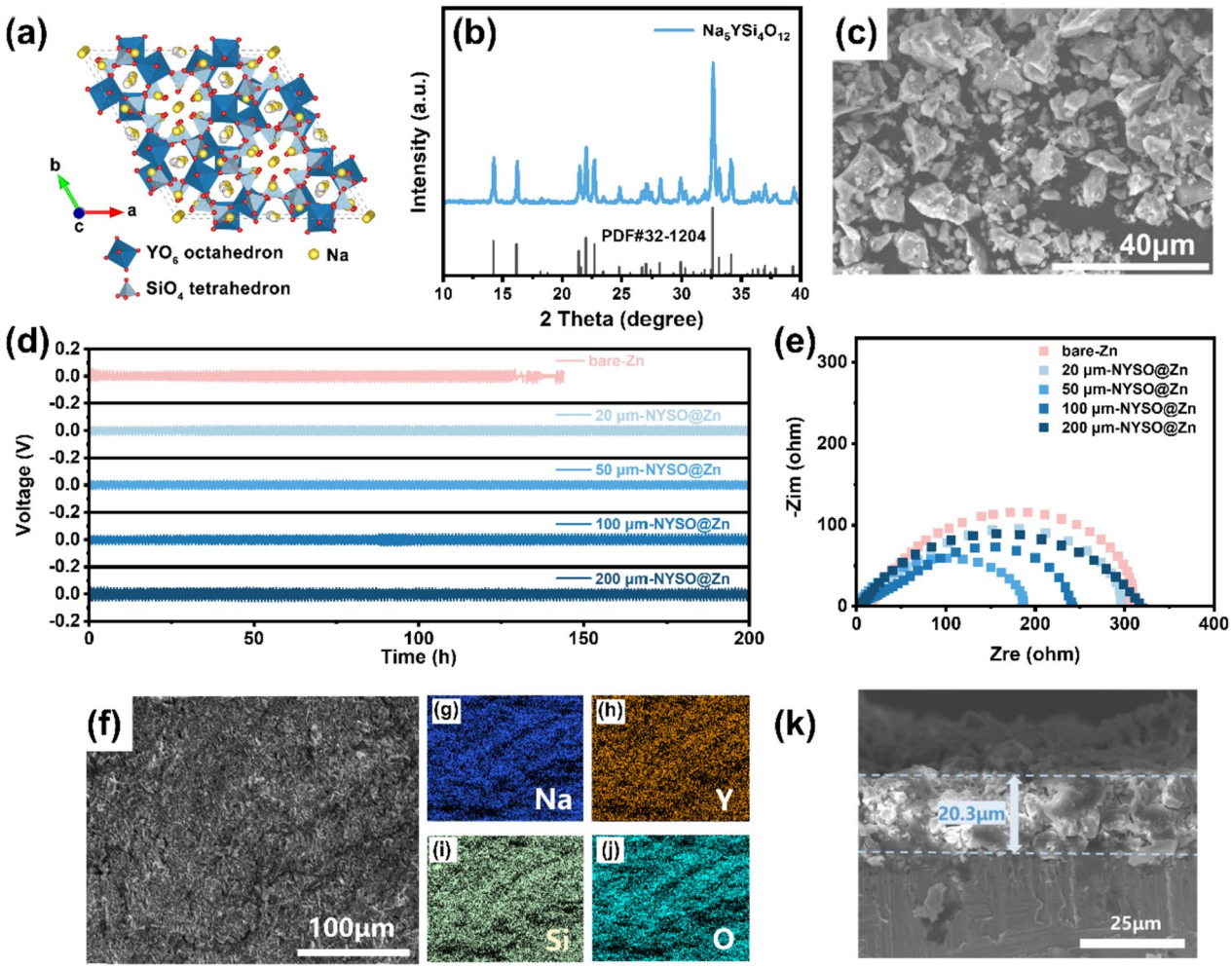

Fig. 1 **a** Schematic crystal structure, **b** XRD pattern, and **c** SEM image of the as-prepared $Na_5Ysi_4O_{12}$ sample; **d** Galvanostatic cycling performances of bare-Zn and different thickness NYSO (i.e., 20 μm, 50 μm, 100 μm, and 200 μm) symmetrical cells at 1 mA cm^{-2} with 1 mAh cm^{-2}. **e** Nyquist plots of NYSO symmetrical cells with different thickness. **f** SEM image of $Na_5Ysi_4O_{12}$ and corresponding element distribution of **g** Na, **h** Y, **i** Si, and **j** O. **k** The cross-sectional SEM of optimal 50 μm-NYSO@Zn electrode

In addition, to explore the electrochemical performance of symmetric cells at high current densities, the rate performance was carried out from 0.2 to 10 mA cm^{-2} with 1 mAh cm^{-2} (Fig. 2c). As expected, the NYSO@Zn anode presents a favorable rate performance with smaller voltage hysteresis at a high current density of 10 mA cm^{-2}, whereas the bare-Zn anode shows severe short-circuit at 1 mA cm^{-2}. The superior cycling life and rate capability can be ascribed to the relatively high Zn^{2+} ionic conductivity of the $Na_5YSi_4O_{12}$ coating with a controllable interface (Figure S6). As calculated from the Nyquist plot (Fig. 2e), the charge transfer resistance of the NYSO@Zn electrode in the initial cycle was obviously lower than that of the Zn foil, indicating an efficient charge transfer kinetics. Upon cycling, the NYSO@Zn electrode exhibits similar impedances after 50 cycles, indicating stable interfacial Zn^{+} conduction. However, a drastic decrease in charge resistance is observed in the bare Zn cell, suggesting a fundamentally altered charge-conduction mechanism called soft shorts [32] (Fig. 2d). In this case, the Zn dendrites cause the small localized electrical connection between two electrodes, which allows the co-existence of direct electron transfer and interfacial reaction, resulting in rapid cell degradation.

Coulombic efficiency (CE), the ratio of the stripping capacity and the plating capacity of the same cycle, is also measured in Cu|bare Zn and Cu|NYSO@Zn cells to evaluate the utilization and sustainability of Zn [33].

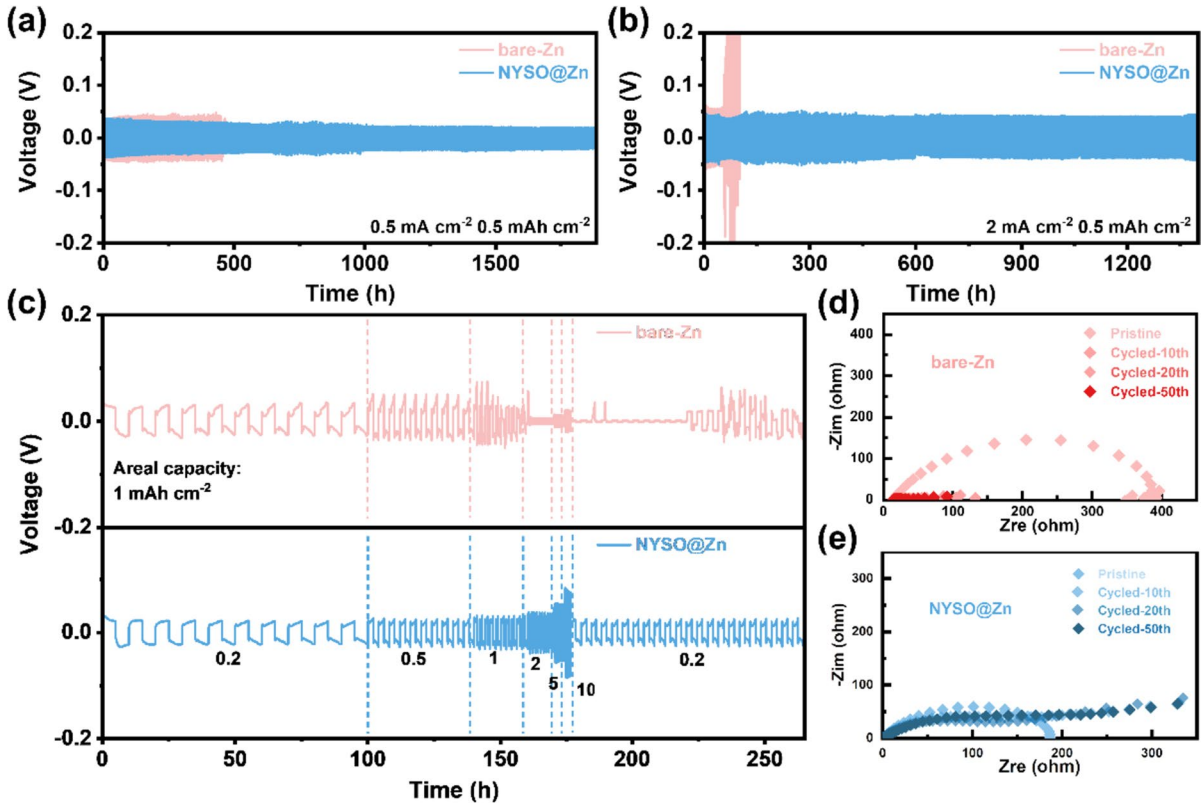

Fig. 2 Long-term cyclability of the bare-Zn and NYSO@Zn symmetric cells at **a** 0.5 mA cm^{-2}/0.5 mAh cm^{-2} and **b** 2 mA cm^{-2}/0.5 mAh cm^{-2}. **c** Rate performances of the Zn symmetric cells from 0.2 to 10 mA cm^{-2}. Nyquist plots of **d** bare-Zn and **e** NYSO@Zn symmetric cells during pristine and various cycling durations

Specifically, the CE measurement is conducted by plating Zn onto a Cu substrate with a capacity of 1.0 mA h cm^{-2} at 1.0 mA cm^{-2}, and then stripping to 0.3 V (Fig. 3a). The Cu|bare Zn cell short-circuit after less than 75 cycles and shows fluctuating CE around 50 cycles, implying severe side reactions on the bare Cu substrate during cycling. For the Cu|NYSO@Zn cell, the CE is remarkably stable up to 138 cycles with a high CE of 99.91%. Indeed, the CE stability of cells with $Na_5YSi_4O_{12}$ protected anodes is significantly enhanced. The corresponding galvanostatic charge/ discharge (GCD) profiles of the bare Zn and NYSO@Zn anodes at 1 mA cm^{-2} are illustrated in Fig. 3b, c. It is found that bare Zn shows a large voltage gap of 73 mV, which falls to 40 mV after 70 cycles. In contrast, lower polarizations of 63 mV at the 1^{st} cycle and 33 mV at the 70^{th} cycle were observed, which confirms that NYSO@Zn could avoid the side reactions and maintain reversible and fast Zn^{2+} kinetics. Apart from this, the nucleation overpotential is further measured to highlight the effect of $Na_5YSi_4O_{12}$ surface coating on Zn deposition. As shown in Figure S7, the nucleation overpotential of bare-Zn reaches as high as 62 mV, higher than that of NYSO@Zn (49 mV) at a current density of 1 mA cm^{-2}. This result indicates that the surface of NYSO coating could prevent the growth of Zn dendrites and modify the homogeneous nucleation with a lower overpotential. The enhanced reaction kinetics with the Zn-Cu asymmetric cells is also discussed by CV testing of NYSO@Zn anode (Fig. 3d). The NYSO@Zn anode shows a higher current, indicating that more active sites on the Zn anode surface achieved faster reaction kinetics, which is in good agreement with the EIS result [34, 35]. The diffusion of Zn^{2+} on the Zn anode continues to deposit continuously at the most favorable nucleation position, and ultimately leads to dendrite forming. The current–time curve may actually reflect the morphological change on the Zn anode along with the electrodeposition process. Therefore, the chronoamperometry (CA) test in Fig. 3e was adopted to analyze the current change of bare Zn and NYSO@Zn anode under -150 mV overpotential within 100 s. The current of bare Zn exhibits a continuous increase within 100 s, indicating the uncontrollable deposition of Zn^{2+}. The adsorbed Zn^{2+} continuously two-dimensional diffuses on Zn anode to achieve the minimization surface

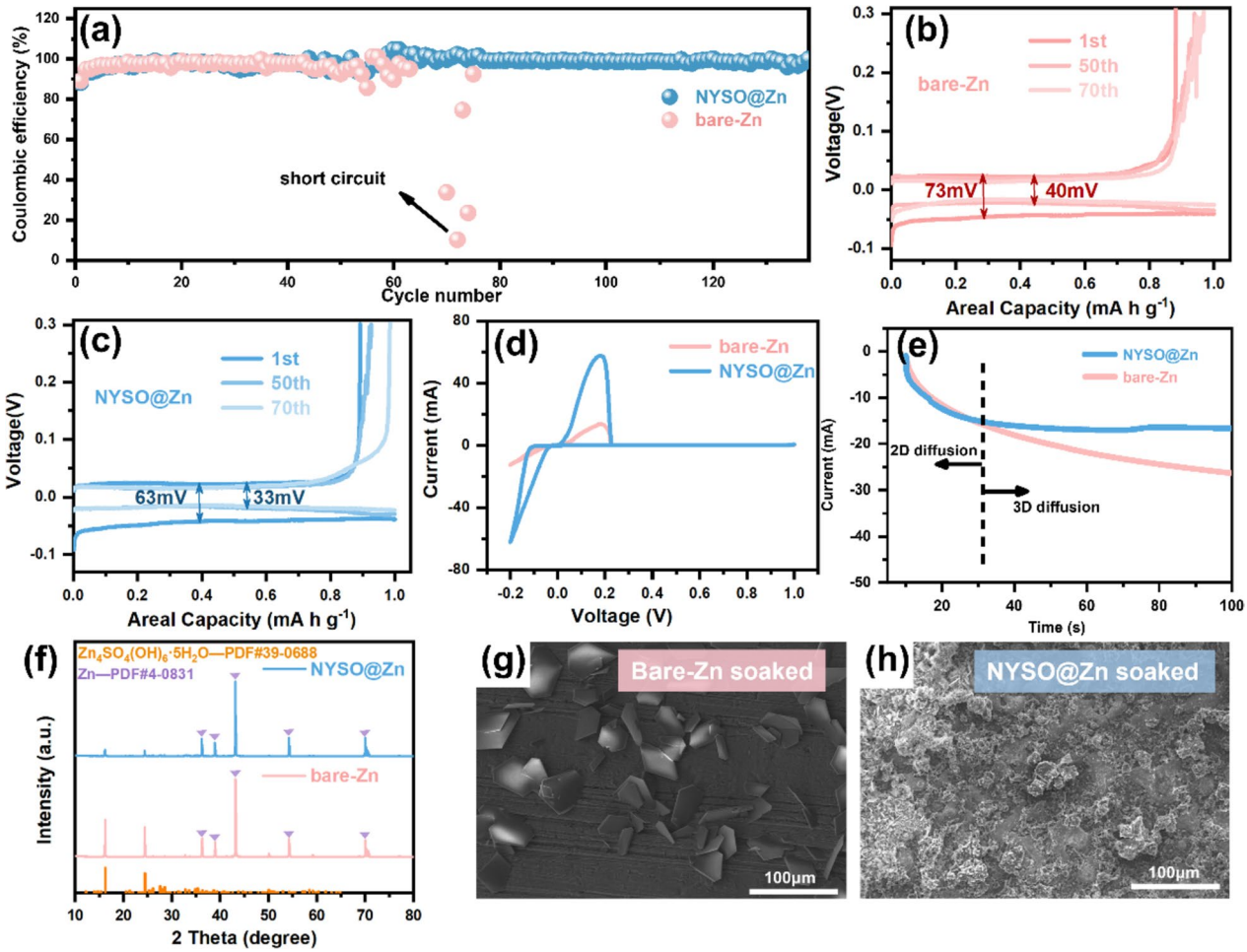

Fig. 3 **a** Coulombic efficiency and corresponding voltage–time curves of **b** Cu|bare Zn and **c** Cu|NYSO@Zn half-cells at 1 mA cm^{-2}. **d** CV and **e** CA curves of Zn nucleation of bare-Zn and NYSO@Zn electrodes at Cu|Zn half-cells and Zn symmetric cells, respectively. **f** XRD pattern of bare-Zn and NYSO@Zn after immersion in 2 M $ZnSO_4$ electrolyte for 7 days and **g**, **h** corresponding evolution of surface morphology

energy, and always deposit on the preferential nucleation position, resulting in the growth of dendrite. Different from bare Zn, the NYSO@Zn anode presents a stable and smaller current in a short time. With the assistance of the NYSO@Zn coating, two-dimensional diffusion is regulated during the process of deposition, so that the Zn^{2+} is uniformly deposited on the Zn anode [36, 37].

To investigate the protective effect of $Na_5YSi_4O_{12}$ coating on Zn metal, we further observe the morphological evolution by SEM and XRD for the bare-Zn and NYSO@Zn in 2 M $ZnSO_4$ electrode after 7 days respectively. For the bare-Zn, newly generated flake by-products, like $ZnSO_4(OH)_6{\cdot}5H_2O$ (Fig. 3f), are found on the surface (Fig. 3g). In comparison with the bare-Zn, the overall morphology of NYSO@Zn remains as is (Fig. 3h), though there are still some minor by-products. In addition, the change of the electrode surface during electrochemical plating of bare-Zn and NYSO@Zn are recorded directly under in-situ optical microscope images. After 5 min of plating at 20 mA cm^{-2}, several protrusions appear on the surface of bare-Zn, indicating a non-uniform Zn plating behavior and the formation of dendritic growth, which becomes more pronounced with increasing reaction time (Fig. 4g). In contrast, the NYSO@Zn electrode shows no significant surface changes even after 30 min, demonstrating the efficiency of the $Na_5YSi_4O_{12}$ layer in inhibiting dendrite growth (Fig. 4h).

The practical use of NYSO@Zn anodes in aqueous ZIBs was further evaluated in full cells. Carbon nanotube (CNT)@MnO_2 composite was used to pair with bare Zn and NYSO@Zn due to the high theoretical capacity and low cost of MnO_2 and the high electronic conductivity of CNT. The X-ray Diffraction (XRD) pattern in Figure S8 shows that all the diffraction peaks match well

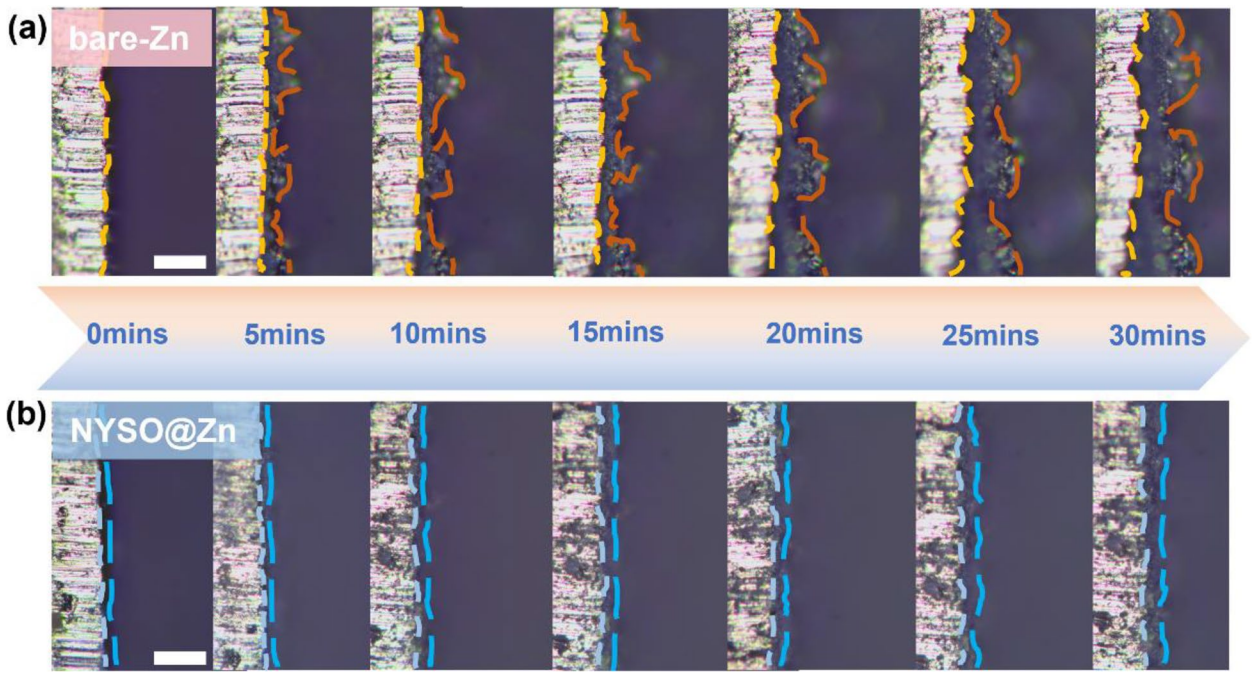

Fig. 4 In-situ optical microscopy images of Zn plating at **a** bare-Zn and **b** NYSO@Zn symmetric transparent cells under current density of 20 mA cm^{-2}. Scale bars: 100 μm

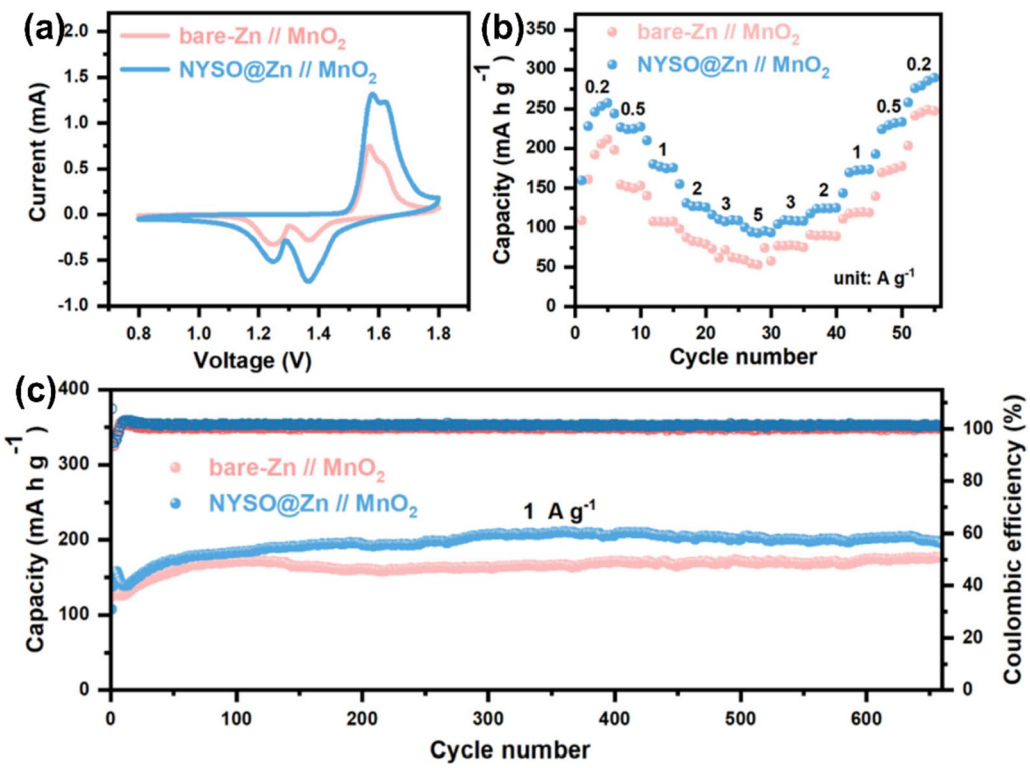

Fig. 5 The electrochemical performance comparisons of bare-Zn|CNT@MnO_2 and NYSO@Zn |CNT@MnO_2 full batteries. **a** CV curves, **b** rate performance from 0.2 to 5 A g^{-1}, and **c** long cycling performance and corresponding coulombic efficiency at 1 A $g.^{-1}$

with MnO_2 (JCPDS PDF 44–0141). As shown in Figure S9, SEM images show a nanotube morphology of CNT@MnO_2 composite. The thermogravimetric analysis (TGA) of the CNT@MnO_2 composite exhibits a 21.15% weight loss in the temperature range from 220 to 700 °C, suggesting a 21.15% weight ratio of CNT (Figure S10). The cyclic voltammetry (CV) profiles of bare Zn/MnO2 and NYSO@Zn|CNT@MnO_2 full cells are illustrated in Fig. 5a within a voltage window of 0.8 to 1.8 V. The two pairs of redox peaks are assigned to the Zn^{2+} insertion and extraction in the CNT@MnO_2 cathode. In the NYSO@Zn|CNT@MnO_2 cells, CV curves demonstrate higher current responses of the redox peaks than that in the bare Zn|MnO_2 cells, implying fast kinetics of Zn deposition/dissolution at NYSO@Zn anode. Figure 5b displays the rate performances of bare Zn|CNT@MnO_2 and NYSO@Zn|CNT@MnO_2 full cells at various current densities. In NYSO@Zn|CNT@MnO_2 cells, discharge capacities of 250 mAh g^{-1}, 224 mAh g^{-1}, 176 mAh g^{-1}, 123 mAh g^{-1}, 107 mAh g^{-1} and 94 mAh g^{-1} were recorded at 0.2 A g^{-1}, 0.5 A g^{-1}, 1 A g^{-1}, 2 A g^{-1}, 3 A g^{-1} and 5 A g^{-1}, respectively. When the current density returns to 0.2 A g^{-1}, NYSO@Zn|CNT@MnO_2 cell still retains a capacity of 280 mA h g^{-1}. The superior rate capability of NYSO@Zn than bare Zn further confirms the rapid Zn^{2+} stripping and plating at the NYSO@Zn interface. Consequently, NYSO@Zn|CNT@MnO_2 cell shows a higher capacity than bare Zn and a long cycling life of 660 cycles at 1 A g^{-1} (Fig. 5c).

3 Conclusions

In summary, we developed a $Na_5YSi_4O_{12}$ protection layer to inhibit the growth of zinc dendrites and stabilize the Zn metal anode. The 20.5 μm thickness of NYSO@Zn anode exhibits a superior lifespan over 1896 cycles at 0.5 mA cm^{-2} in symmetrical batteries. Meanwhile, the NYSO@Zn anode presents a favorable rate performance at a high current density of 10 mA cm^{-2}. Additionally, the $Na_5YSi_4O_{12}$ coating can successfully reduce the generation of by-products and prevent dendrites growth on the Zn metal anode/electrolyte interface. Consequently, this simple strategy enables the NYSO@Zn|CNT@MnO_2 cell with a higher capacity and stability than bare Zn.

Abbreviations

AZIBs	Aqueous zinc-ion batteries
NYSO	$Na_5YSi_4O_{12}$
SHE	Standard hydrogen electrode
CE	Coulombic efficiency
NTP	$NaTi_2(PO_4)_3$
GCD	Galvanostatic charge/ discharge
CV	Cyclic voltammetry
CA	Chronoamperometry
XRD	X-ray Diffraction

Supplementary Information

The online version contains supplementary material available at https://doi.org/10.1007/s43979-023-00073-5.

Additional file 1: Figure S1. The polarization voltage of bare-Zn and different thickness NYSO (i.e., 20 μm, 50 μm, 100 μm, and 200 μm) symmetrical cells at 1 mA cm^{-2} with 1 mAh cm^{-2}. **Figure S2.** Long-term cyclability of the bare-Zn and NYSO@Zn symmetric cells at 1 mA cm^{-2}/0.5 mAh cm^{-2}. **Figure S3.** SEM images of bare Zn and NYSO@Zn electrodes before cycling and after 100 cycles at 1 mA cm^{-2}/1 mAh cm^{-2}. **Figure S4.** Long-term cyclability of the bare-Zn and NYSO@Zn symmetric cells at 5 mA cm^{-2}/0.5 mAh cm^{-2}. **Figure S5.** The enlarged voltage-time curves of NYSO@Zn and bare Zn symmetric cells at (a) 0.5 mA cm^{-2}/0.5 mAh cm^{-2} and (b) 2 mA cm^{-2}/0.5 mAh cm^{-2}. **Figure S6.** The EIS spectra of (a) Ti symmetric cell with glass fiber and (b) NYSO coated Ti symmetric cell with glass fiber. **Figure S7.** Nucleation overpotential of bare-Zn and NYSO@Zn at 1 mA cm^{-2}. **Figure S8.** XRD pattern of the as-prepared CNT/MnO_2 sample. **Figure S9.** SEM image of the as-prepared CNT/MnO_2 sample. **Figure S10.** TGA curve of the as-prepared CNT/MnO_2 sample.

Acknowledgements

This work was supported by National Natural Science Foundation of China with Grant No. 12274176 and 51972142. We also would like to thank the support from the Fundamental Research Funds for the Center Universities, and Department of Science and Technology of Jilin Province with Grant No. 20220201118GX.

Authors' contributions

SY, NC, and FD conceived the project; NX and GS performed the experiment; NX, CY, and SY analyzed the data; SY and FD wrote and revised the manuscript; All authors read and approved the final manuscript. NC and CY contributed equally to this work.

Funding

Open access funding provided by Shanghai Jiao Tong University. Open access funding provided by Jilin University. This work was supported by National Natural Science Foundation of China with Grant No. 12274176 and 51972142. We also would like to thank the support from the Fundamental Research Funds for the Center Universities, and Department of Science and Technology of Jilin Province with Grant No. 20220201118GX.

Availability of data and materials

The datasets generated during and/or analysed during the current study are available from the corresponding author on reasonable request.

Declarations

Ethics approval and consent to participate

Not applicable.

Consent for publication

Not applicable.

Competing interests

The authors have no competing interests to declare that are relevant to the content of this article.

Received: 8 August 2023 Revised: 2 October 2023 Accepted: 6 November 2023
Published online: 01 December 2023

References

1. Zhang N, Chen X, Yu M, Niu Z, Cheng F, Chen J (2020) Materials chemistry for rechargeable zinc-ion batteries. Chem Soc Rev 49:4203–4219. https://doi.org/10.1039/c9cs00349e

2. Zhang Q, Luan J, Tang Y, Ji X, Wang H (2020) Interfacial design of dendrite-free zinc anodes for aqueous zinc-ion batteries. Angew Chem Int Ed Engl 59:13180–13191. https://doi.org/10.1002/anie.202000162
3. Zou Y, Yang X, Shen L, Su Y, Chen Z, Gao X, Zhou J, Liang S (2022) Emerging strategies for steering orientational deposition toward high-performance Zn metal anodes. Energy Environ Sci 15:5017–5038. https://doi.org/10.1039/d2ee02416k
4. Du W, Ang E, Yang Y, Zhang Y, Ye M, Li C (2020) Challenges in the material and structural design of zinc anode towards high-performance aqueous zinc-ion batteries. Energy Environ Sci 15:5017–5038. https://doi.org/10.1039/D0EE02079F
5. Lv Y, Zhao M, Du Y, Kang Y, Xiao Y, Chen S (2022) Engineering a self-adaptive electric double layer on both electrodes for high-performance zinc metal batteries. Energy Environ Sci 15:4748–4760. https://doi.org/10.1039/D2EE02687B
6. Han C, Li W, Liu H, Dou S, Wang J (2020) Principals and strategies for constructing a highly reversible zinc metal anode in aqueous batteries. Nano Energy 74:104880. https://doi.org/10.1016/j.nanoen.2020.104880
7. Geng Y, Pan L, Peng Z, Sun Z, Lin H, Mao C, Wang L, Dai L, Liu H, Pan K, Wu X, Zhang Q, He Z (2022) Electrolyte additive engineering for aqueous Zn ion batteries. Energy Storage Mater 51:733–755. https://doi.org/10.1016/j.ensm.2022.07.017
8. Qian G, Zan G, Li J, Lee S, Wang Y, Zhu Y, Gul S, Vine D, Lewis S, Yun W, Ma Z, Pianetta P, Lee J, Li L, Liu Y (2022) Structural, dynamic, and chemical complexities in zinc anode of an operating aqueous Zn-ion battery. Adv Energy Mater 12:2200255. https://doi.org/10.1002/aenm.202200255
9. Cai Z, Ou Y, Wang J, Xiao R, Fu L, Yuan Z, Zhan R, Sun Y (2020) Chemically resistant Cu-Zn/Zn composite anode for long cycling aqueous batteries. Energy Storage Mater 27:205–211. https://doi.org/10.1016/j.ensm.2020.01.032
10. Yuan C, Yin L, Du P, Yu Y, Zhang K, Ren X, Zhan X, Gao S (2022) Micro-groove-patterned Zn metal anode enables ultra-stable and low-over-potential Zn deposition for long-cycling aqueous batteries. Chem Eng J 442:136231. https://doi.org/10.1016/j.cej.2022.136231
11. Bayaguud A, Fu Y, Zhu C (2022) Interfacial parasitic reactions of zinc anodes in zinc ion batteries: Underestimated corrosion and hydrogen evolution reactions and their suppression strategies. J Energy Chem 64:246–262. https://doi.org/10.1016/j.jechem.2021.04.016
12. Zhang Q, Luan J, Huang X, Zhu L, Tang Y, Ji X, Wang H (2020) simultaneously regulating the ion distribution and electric field to achieve dendrite-free Zn anode. Small 16:2000929. https://doi.org/10.1002/smll.202000929
13. Yi Z, Liu J, Tan S, Sang Z, Mao J, Yin L, Liu X, Wang L, Hou F, Dou S, Cheng H-M, Liang J (2022) An ultrahigh rate and stable zinc anode by facet-matching-induced dendrite regulation. Adv Mater 34:2203835. https://doi.org/10.1002/adma.202203835
14. Cao Q, Gao H, Gao Y, Yang J, Li C, Pu J, Du J, Yang J, Cai D, Pan Z, Guan C, Huang W (2021) Regulating dendrite-free zinc deposition by 3D zincophilic nitrogen-doped vertical graphene for high-performance flexible Zn-ion batteries. Adv Funct Mater 31:2103922. https://doi.org/10.1002/adfm.202103922
15. Hu Z, Zhou L, Meng D, Zhao L, Wang W, Li Y, Huang Y, Wu Y, Yang S, Li L, Hong Z (2023) Surface Engineering for Ultrathin Metal Anodes Enabling High-Performance Zn-ion batteries. ACS Appl Mater Interfaces 15:5161–5171. https://doi.org/10.1021/acsami.2c18836
16. Hao J, Yuan L, Ye C, Chao D, Davey K, Guo Z, Qiao S (2021) Boosting zinc electrode reversibility in aqueous electrolytes by using low-cost antisolvents. Angew Chem Int Ed Engl 60:7366–7375. https://doi.org/10.1002/anie.202016531
17. Qin H, Kuang W, Hu N, Zhong X, Huang D, Shen F, Wei Z, Huang Y, Xu J, He H (2022) Building metal-molecule interface towards stable and reversible Zn metal anodes for aqueous rechargeable zinc batteries. Adv Funct Mater 32:2206695. https://doi.org/10.1002/adfm.202206695
18. Qiu M, Sun P, Ai Q, Cui G, Mai W (2022) Metal-coordination chemistry guiding preferred crystallographic orientation for reversible zinc anode. Energy Storage Mater 49:463–470. https://doi.org/10.1016/j.ensm.2022.04.018
19. Zhu Y, Hoh H, Qian S, Sun C, Wu Z, Huang Z, Wang L, Batmunkh M, Lai C, Zhang S, Zhong Y (2022) Ultrastable zinc anode enabled by CO_2-induced interface layer. ACS Nano 16:14600–14610. https://doi.org/10.1021/acsnano.2c05124
20. Yuan C, Liu C, Li X, Zhi Y, Zhan X, Gao S (2023) A facile candle-soot nanoparticle decoration enables dendrite-free Zn anodes for long-cycling aqueous batteries. ACS Appl Energy Mater 6:1897–1905. https://doi.org/10.1021/acsaem.2c03838
21. Ao C, Zhao C, Guo Z, Lu X, Liu N, Zhang Y, Fan L, Zhang N (2022) Fast-growing multifunctional $ZnMoO_4$ protection layer enable dendrite-free and hydrogen-suppressed Zn anode. Energy Storage Mater 44:353–359. https://doi.org/10.1016/j.ensm.2021.10.016
22. Yang J, Yin B, Sun Y, Pan H, Sun W, Jia B, Zhang S, Ma T (2022) Zinc anode for mild aqueous zinc-ion batteries: challenges, strategies, and perspectives. Nanomicro Lett 14:42. https://doi.org/10.1007/s40820-021-00782-5
23. Kang L, Cui M, Jiang F, Gao Y, Luo H, Liu J, Liang W, Zhi C (2018) Nanoporous $CaCO_3$ coatings enabled uniform Zn stripping/plating for long-life zinc rechargeable aqueous batteries. Adv Energy Mater 8:1801090. https://doi.org/10.1002/aenm.201801090
24. Liang P, Yi J, Liu X, Wu K, Wang Z, Cui J, Liu Y, Wang Y, Xia Y, Zhang J (2020) Highly reversible Zn anode enabled by controllable formation of nucleation sites for Zn-based batteries. Adv Funct Mater 30:1908528. https://doi.org/10.1002/adfm.201908528
25. Deng C, Xie X, Han J, Tang Y, Gao J, Liu C, Shi X, Zhou J, Liang S (2020) A sieve-functional and uniform-porous kaolin layer toward stable zinc metal anode. Adv Funct Mater 30:2000599. https://doi.org/10.1002/adfm.202000599
26. Hong L, Wu X, Ma C, Huang W, Zhou Y, Wang K-X, Chen J-S (2021) Boosting the Zn-ion transfer kinetics to stabilize the Zn metal interface for high-performance rechargeable Zn-ion batteries. J Mater Chem A 9:16814–16823. https://doi.org/10.1039/d1ta03967a
27. Yang Y, Liu C, Lv Z, Yang H, Cheng X, Zhang S, Ye M, Zhang Y, Chen L, Zhao J, Li C (2021) Redistributing Zn-ion flux by interlayer ion channels in Mg-Al layered double hydroxide-based artificial solid electrolyte interface for ultra-stable and dendrite-free Zn metal anodes. Energy Storage Mater 41:230–239. https://doi.org/10.1016/j.ensm.2021.06.002
28. Zhao K, Wang C, Yu Y, Yan M, Wei Q, He P, Dong Y, Zhang Z, Wang X, Mai L (2018) Ultrathin surface coating enables stabilized zinc metal anode. Adv Mater Interfaces 5:1800848. https://doi.org/10.1002/admi.201800848
29. Hao J, Li B, Li X, Zeng X, Zhang S, Yang F, Liu S, Li D, Wu C, Guo Z (2020) An in-Depth study of Zn metal surface chemistry for advanced aqueous Zn-ion batteries. Adv Mater 32:2003021. https://doi.org/10.1002/adma.202003021
30. Cao Z, Zhu X, Xu D, Dong P, Chee M, Li X, Zhu K, Ye M, Shen J (2021) Eliminating Zn dendrites by commercial cyanoacrylate adhesive for zinc ion battery. Energy Storage Mater 36:132–138. https://doi.org/10.1016/j.ensm.2020.12.022
31. Liu M, Cai J, Ao H, Hou Z, Zhu Y, Qian Y (2020) $NaTi_2(PO_4)_3$ solid-state electrolyte protection layer on Zn metal anode for superior long-life aqueous zinc-ion batteries. Adv Funct Mater 30:2004885. https://doi.org/10.1002/adfm.202004885
32. Li Q, Chen A, Wang D, Pei Z, Zhi C (2022) "Soft shorts" hidden in zinc metal anode research. Joule 6:273–279. https://doi.org/10.1016/j.joule.2021.12.009
33. Xie D, Wang Z-W, Gu Z-Y, Diao W-Y, Tao F-Y, Liu C, Sun H-Z, Wu X-L, Wang J-W, Zhang J-P (2022) Polymeric molecular design towards horizontal Zn electrodeposits at constrained 2D Zn^{2+} diffusion: dendrite-free Zn anode for long-life and high-rate aqueous zinc metal battery. Adv Funct Mater 32:2204066. https://doi.org/10.1002/adfm.202204066
34. Zhu X, Li X, Essandoh M, Tan J, Cao Z, Zhang X, Dong P, Ajayan P, Ye M, Shen J (2022) Interface engineering with zincophilic MXene for regulated deposition of dendrite-free Zn metal anode. Energy Storage Mater 50:243–251. https://doi.org/10.1016/j.ensm.2022.05.022
35. Zhang N, Huang S, Yuan Z, Zhu J, Zhao Z, Niu Z (2021) Direct self-assembly of MXene on Zn anodes for dendrite-free aqueous zinc-ion batteries. Angew Chem Int Ed Engl 60:2861–2865. https://doi.org/10.1002/anie.202012322
36. Zhang Y, Han X, Liu R, Yang Z, Zhang S, Zhang Y, Wang H, Cao Y, Ai C, Sun J (2022) Manipulating the zinc deposition behavior in hexagonal patterns at the preferential Zn (100) crystal plane to construct surficial dendrite-free zinc metal anode. Small 18:2105978. https://doi.org/10.1002/smll.202105978
37. Zhou S, Wang Y, Lu H, Zhang Y, Fu C, Usman I, Liu Z, Feng M, Fang G, Cao X, Liang S, An P (2021) Anti-corrosive and Zn-ion-regulating composite interlayer enabling long-life Zn metal anodes. Adv Funct Mater 31:2104361. https://doi.org/10.1002/adfm.202104361

Publisher's Note